Evaluating the Correspondence Between Signal-Based Modes and Linearized Eigenmodes in a Large-Scale Power-System

Owen S. Cornmesser, Adam B. Birchfield, Thomas J. Overbye
Department of Electrical and Computer Engineering
Texas A&M University
College Station, Texas
{ocornmesser, abirchfield, overbye}@tamu.edu

***Abstract*—As power systems become increasingly dynamic and complex, accurate characterization of system-wide oscillatory modes is essential for system planning, operation, and control. The modes identified through a signal-based approach are often interpreted as direct representations of the underlying eigenmodes of the linearized system, yet their frequency, damping, and mode shape may not always correspond to individual linearized modes in large-scale power systems. To evaluate this correspondence, this paper analytically linearizes a detailed 4745-state model of the 2000-bus Texas synthetic grid and compares its eigenmodes with modes identified from nonlinear ringdown simulations. Results show that some distinct, individual system-wide eigenmodes are consistently identified by the signal-based approach, whereas many signal-based modes do not correspond to an individual eigenmode despite accurate time-domain reconstruction from both modal representations. These results suggest that care should be taken when assigning meaning to signal-based modes, as the correspondence between them and underlying eigenmodes may not always hold.**

***Index Terms*—Signal-based modal analysis, model-based modal analysis, inter-area oscillations, small-signal stability**

I. Introduction

The increasing dynamic complexity within large-scale systems is bringing system-wide oscillations, which can be detrimental to device lifespan and can introduce reliability risks if they are poorly damped. For this reason, these oscillations (also referred to as "modes") are closely tracked, studied, and analyzed in systems such as the Western Interconnection [1], [2] and the Eastern Interconnection [3], [4]. Understanding how these observed modes relate to the underlying dynamic system is increasingly important as changing generation dispatch, inverter-based resources, large load interconnection requests, and evolving control structures are beginning to alter system oscillatory behavior. Detailed models and methodologies are crucial, including those that can characterize the system either analytically or through a data-driven approach.

On the analytical side, the well-established small-signal stability theory is often used. Here, the nonlinear differential-algebraic equations describing the system are linearized about an equilibrium operating point, and the resultant eigenvalues and right eigenvectors of the corresponding state matrix characterize the natural modes of the system [5]. This framework also enables calculation of quantities such as participation factors, eigenvalue sensitivities, modal residues, controllability, and observability. In small and moderate-size systems, the relevant modes can often be directly computed, visualized, and interpreted. In realistic large-scale systems, however, detailed linearization may not be feasible as many internal device controls and parameters are hidden behind vendor black-box models, and the size of the state matrix may be computationally infeasible for diagonalization.

For these reasons, signal-based modal analysis is widely used for real-world oscillation monitoring and analysis. Signal-based methods fit a summation of exponentially damped sinusoids to data; they do not require complete knowledge of the physical system model and can be applied directly to PMU and other synchrophasor measurements. However, a key limitation is that the connection between these computed modes and physical device parameters, state variables, or linearized modes is not always straightforward.

Modes from a signal-based approach have long been interpreted as realizations of the linearized system modes. This comparison is natural as the signal-based approach computes the best-fit set of exponentially damped sinusoids to the data, which is mathematically similar to the modal representation of the linearized system. However, low error in the fitting process does not, by itself, establish that each mode from the signal-based analysis corresponds one-to-one with a single mode of the linearized model.

This interpretation is called into question by observed behavior in which the modes from a signal-based approach appear to change, in terms of frequency, damping, and mode shape [6], [7] across disturbances. This is in contrast to modes from linearization, which, for a fixed topology and model, are dependent only on the operating point. Further clarity is needed on the origin of signal-based modes, and what conditions are necessary for signal-based modes to align with the linearized system modes. Such a comparison is difficult in large-scale systems because a detailed analytical eigenstructure is rarely available. This paper addresses this gap by analytically linearizing a large-scale power system and comparing these modes to those obtained from a signal-based approach. Successive disturbances are applied throughout the system to evaluate how the signal-based modes change relative to the underlying linearized modes. The contributions of this

Copyright ©2026 IEEE. Personal use of this material is permitted. From the North American Power Symposium (NAPS) 2026, Houghton, MI, October 2026

paper can be summarized as follows:

- This paper analytically linearizes a detailed 4745-state power-system model, providing a neccessary reference for evaluating signal-based modes.
- This paper demonstrates that in this large-scale system, some system-wide signal-based modes are consistently observed, and they correspond strongly to individual linearized modes.
- In contrast, this paper shows that there are signal-based modes that do not correspond to individual linearized modes, even though both modal representations reconstruct the same time-domain response.

The results highlight an important limitation in interpreting signal-based modes as direct representations of the system's underlying linearized modes, even though both exhibit the same oscillatory time-domain behavior.

II. Background and Problem Setup

Throughout this paper, modes obtained from the linearized system model will be referred to as MBEs, short for model-based eigenmodes. The modes identified from a signal-based method will be referred to as SBMs, short for signal-based modes.

A. Model-Based Modal Representation

In a dynamic power system of arbitrary size, the dynamic devices are represented by a nonlinear differential-algebraic model of the form

$$\dot{x} = f(x, v), \qquad i = g(x, v), \qquad i = \mathrm{Y}v \tag{1}$$

where, with n_x dynamic states and n_b buses in the network, $x \in \mathbb{R}^{n_x}$ is the vector of system states, $v \in \mathbb{C}^{n_b}$ is the vector of system bus voltage phasors, $i \in \mathbb{C}^{n_b}$ is the vector of system bus current injection phasors, $f(\cdot)$ and $g(\cdot)$ are nonlinear vector functions, and $\mathrm{Y} \in \mathbb{C}^{n_b \times n_b}$ is the network admittance matrix. With no forcing input, (1) may be linearized about a fixed operating point, with the algebraic variables eliminated, and reduced to the state-space form

$$\Delta\dot{x} = \mathrm{A}_{sys}\Delta x. \tag{2}$$

Assuming A_{sys} is diagonalizable and has distinct eigenvalues, the linearized state response following a disturbance can be expressed as

$$\Delta x_{lin}^{(r)}(t) = \sum_{j=1}^{n_x} c_j^{(r)} v_j e^{\lambda_j t}, \tag{3}$$

where r indexes the initiating disturbance, $\lambda_j \in \mathbb{C}$ is the jth eigenvalue of A_{sys}, $v_j \in \mathbb{C}^{n_x}$ is the corresponding right eigenvector, and $c_j^{(r)} \in \mathbb{C}$ is the modal coefficient for disturbance r. If $\mathrm{V} := [v_1\ v_2\ \ldots\ v_{n_x}]$, then the coefficient vector is $c^{(r)} = \mathrm{V}^{-1}\Delta x^{(r)}(0)$.

Note that the eigenvalues λ_j and eigenvectors v_j are fixed by the operating point, topology, and dynamic model parameterization. Therefore, for sufficiently small topology-preserving disturbances, the *MBEs do not change with the disturbance*. Changing the disturbance r changes the relative excitation of the MBEs, but not the MBEs themselves.

B. Signal-Based Modal Representation

In this analysis, the matrix pencil method [8] is used as the example signal-based technique. With a subset of system state variables during a ringdown response, the data are fit to

$$\widehat{\Delta x_{mp}}^{(r)}(t) = d^{(r)}(t) + \sum_{i=1}^{n_{mp}} \alpha_i^{(r)} e^{\sigma_i^{(r)} t} \cos\left(\omega_i^{(r)} t + \phi_i^{(r)}\right), \tag{4}$$

where n_{mp} is the number of extracted SBMs, $d^{(r)}(t) \in \mathbb{R}^{\ell}$ is a detrending term, $\sigma_i^{(r)} \in \mathbb{R}$ is the exponential decay rate, $\omega_i^{(r)} \in \mathbb{R}$ is the oscillatory frequency, and $\alpha_i^{(r)}, \phi_i^{(r)} \in \mathbb{R}^{\ell}$ describe the magnitude and phase of the component across the ℓ signals, respectively. Equivalently, and without the detrending term, the oscillatory content of the time-domain data may be written in complex form as

$$\widehat{\Delta x_{mp,osc}}^{(r)}(t) = \sum_{i=1}^{n_{mp}} \widehat{\beta}_i^{(r)} e^{\widehat{\lambda}_i^{(r)} t}, \tag{5}$$

where $\widehat{\lambda}_i^{(r)} = \widehat{\sigma}_i^{(r)} + \mathrm{j}\widehat{\omega}_i^{(r)}$ is the ith SBM pole, $\widehat{\beta}_i^{(r)} = \alpha_i^{(r)} \angle \phi_i^{(r)} \in \mathbb{C}^{\ell}$ is the corresponding SBM shape across the signal data, and n_{mp} is the number of extracted SBMs.

The matrix pencil method first forms the poles $\widehat{z}_i^{(r)}$ through block-Hankel matrices from the sampled data, then applies a truncated singular-value decomposition (SVD), and solves the resulting generalized eigenvalue problem. Further details of the estimator used in this paper can be found in [9], which is a variation named the iterative matrix pencil (IMP) method.

C. Problem Statement

Assume a nonlinear time integration is conducted on (1); a small, topology-preserving disturbance is simulated, and the system is allowed to ring down back to equilibrium. The nonlinear state vector during the disturbance is recorded as $x_{nl}^{(r)}(t)$, and the signal-based method is applied to these data. If the subsequent reconstruction of both (3) and (5) represents $\Delta x_{nl}^{(r)}(t)$ with low error, then the system is well represented by a summation of exponentially damped sinusoids, and the following is satisfied:

$$\Delta x_{nl}^{(r)}(t) \approx \Delta x_{lin}^{(r)}(t) \approx \widehat{\Delta x_{mp}}^{(r)}(t) \tag{6}$$

Not considering detrending and focusing only on the oscillatory content, (6) can be expressed as follows:

$$\sum_{j \in \Phi} c_j^{(r)} v_j e^{\lambda_j t} \approx \sum_{i=1}^{n_{mp}} \widehat{\beta}_i^{(r)} e^{\widehat{\lambda}_i^{(r)} t}. \tag{7}$$

Here, Φ is the set of eigenmodes with a nonzero imaginary part, i.e., oscillatory eigenmodes. A common implicit assumption of (7) is that each SBM on the right corresponds to an individual MBE on the left. However, there is no inherent guarantee that this will occur, especially in large-scale systems where the number of identified modes n_{mp} is much smaller than the number of system states n_x. Note that the constant term $c_j^{(r)}$ does not affect the relative phasing and magnitude

within elements of v_j, and therefore the observed relative phasing and magnitude within $\widehat{\beta_i^{(r)}}$ will remain the same across values of $c_j^{(r)}$ if the SBM corresponds to a single MBE.

The objective of this paper is to shed light on the question: *do signal-based modes that accurately reconstruct the time-domain signal necessarily correspond one-to-one with model-based eigenmodes?* This is assessed through multiple ringdown simulations by evaluating modal similarity in each case. Correspondence is evaluated using frequency, damping, mode shape, and time-domain reconstruction accuracy.

III. Assessing Correspondence Between Signal-Based Modes and Eigenmodes

The question of whether an SBM corresponds to a single MBE, or does not, can be assessed by comparing an SBM pole and shape against several MBE eigenvalue and eigenvector pairs, as well as confirming that both reconstruct with low error to the simulated time-domain data. This section outlines how the similarities are computed in this paper.

A. Reconstruction

The SBMs are computed so that they reconstruct with low error relative to the original time-domain data through (5). Likewise, the MBE expression in (3) has a similar modal structure, which is why the signal-based approach may estimate the MBEs of the system. Using this relationship, the eigenvalues and eigenvectors of the MBEs can be used to compute the time-domain response given the initial perturbation $\Delta x^{(r)}(0)$. The reconstruction error between (5) and (3) is important because it indicates whether it is meaningful to assess their modal correspondence; if they are not nearly equivalent, their modal similarity cannot be meaningfully assessed from the response. For use in (3), the perturbation vector is computed via

$$\Delta x^{(r)}(0) = x_{nl}^{(r)}(t_+) - x_{nl}^{(r)}(t_-), \tag{8}$$

where t_+ is the time step immediately after the disturbance clearing time, and t_- is the time directly before the disturbance being applied, i.e., the equilibrium point. The normalized root-mean-squared-error (NRMSE) for each signal is evaluated for both the linear model reconstruction, $\Delta x_{lin}^{(r)}(t)$, and the signal-based reconstruction, $\Delta x_{mp}^{(r)}(t)$, and is calculated as

$$\mathrm{NRMSE} = 100\% \times \frac{\mathrm{RMS}(\Delta x_{est}^{(r)}(t) - \Delta x_{nl}^{(r)}(t))}{\max(\Delta x_{nl}^{(r)}(t)) - \min(\Delta x_{nl}^{(r)}(t))}, \tag{9}$$

where $\Delta x_{est}^{(r)}(t)$ is either $\Delta x_{lin}^{(r)}(t)$ or $\Delta x_{mp}^{(r)}(t)$. With low NRMSE, the similarity between the SBMs and MBEs is assessed using frequency, damping, and mode-shape.

B. Frequency, Damping and Eigenvalue

For an eigenvalue λ_i, the modal frequency f_i and damping ratio ζ_i are

$$f_i = \frac{|\operatorname{Im}(\lambda_i)|}{2\pi}, \qquad \zeta_i = \frac{-\operatorname{Re}(\lambda_i)}{|\lambda_i|}. \tag{10}$$

Observation of similar frequency and damping is a necessary indicator that an SBM corresponds to a single MBE. Here, the frequency and damping of the eigenvalues are considered when matching with SBMs. However, in large-scale power systems, using only frequency and damping may not be sufficient given the large number of MBEs, as several MBEs may be closely matched in frequency and damping.

C. Mode Shape and Right Eigenvector

To provide additional clarity, the corresponding eigenvector, v_i, of each eigenvalue is compared to the SBM shape to determine whether a distinct match arises. This paper uses the Modal Assurance Criterion (MAC) to compare the mode shape from the SBM to the right eigenvector of an MBE. This quantity is referred to as the Complex Modal Assurance Criterion (CMAC) or MACX when it is applied to complex modes [10]. CMAC is computed via

$$\mathrm{CMAC}_{ij}^{(r)} = \frac{\left|\left(\widehat{\beta}_i^{(r)}\right)^H v_j^g\right|^2}{\left(\left(\widehat{\beta}_i^{(r)}\right)^H \widehat{\beta}_i^{(r)}\right)\left((v_j^g)^H v_j^g\right)}, \tag{11}$$

where H is the conjugate transpose. The recorded signals in this study are limited to the generator speed state variables. Therefore, the MBE eigenvectors are restricted to their generator speed entries before computing CMAC, producing v_j^g. This ensures both vectors have the same dimension and compares only the signals available to the signal-based analysis. A CMAC near one indicates that the two vectors span nearly the same direction, up to scale and phase. A value near zero indicates that the two vectors are nearly orthogonal, i.e., they do not have the same shape. If an SBM aligns well with a single MBE with respect to frequency, damping, and mode shape, it provides evidence that the SBM primarily represents that MBE.

IV. Test System and Analysis Procedure

A. System Under Study

The case study uses the 2000-bus Texas Synthetic Grid [11] to compare MBE and SBM representations because it contains a nontrivial number of underlying MBEs. The dynamic case contains 432 online generators represented by GENROU machine models, IEEET1 exciter models, and TGOV1 governor models. The analytical linearization yields 4745 retained dynamic states after eliminating states associated with limits or zero time constants. The use of detailed machine, governor, and exciter models in a full analytical linearization provides a detailed set of MBEs and, to the authors' knowledge, a rare large-scale analytical MBE reference in the literature.

B. Ringdown Simulations and Matrix Pencil Implementation

Nonlinear time-domain simulations are performed in PowerWorld Simulator. Each disturbance is a three-phase-to-ground self-clearing fault applied at $t = 1$ s and cleared at $t = 1.01$ s. The fault is topology-preserving so that the post-fault response can be compared with the same pre-fault linearization. The short clearing time is chosen to create a small perturbation

therefore better preserve the relevance of the local linear model.

The signal-based modal analysis of the nonlinear time-domain data uses the IMP implemented in PowerWorld Simulator. The input signals are generator speeds over the window from $t = 1.05$ s to $t = 19$ s, the number of iterations is 20, and the maximum frequency used for down-sampling is 5 Hz. The SVD threshold is set to PowerWorld's default of 0.025. These settings are held constant across all disturbances to avoid confusing disturbance effects with estimator-setting effects.

C. Analytical Linearization

The model-based linearization follows the analytical small-signal formulation of [5]. The Jacobian matrices are computed *analytically* from the dynamic device differential equations. MATLAB and the Symbolic Toolbox are used to define the equations and compute the local derivatives used in the Jacobians. The power flow solution is then used to evaluate these matrices numerically. Finally, the device Jacobians and network admittance matrices are connected to form the system-wide state-space model. The eigenvalues and eigenvectors of A_{sys} are then computed using the MATLAB command `eig`. The validity of this process is assessed through reconstruction using (3); the eigenvalues, eigenvectors, and initial state perturbation vector are used to compute the time-domain trajectory, and the result is compared to the nonlinear time-domain simulation data using (9).

V. Large-Scale Case Study Results

This section compares the SBMs to the MBEs for the large-scale system under study. A single disturbance is examined first, highlighting where matches and mismatches occur. The tested fault location is then varied across 28 zones in the system to evaluate whether the matches and mismatches persist in the same way. The time-domain reconstruction is computed for both modal representations, assessing the validity of the MBEs and the expression in (7).

A. Results from an Initial Disturbance

The initial disturbance is applied near the center of the system at the 115 kV level. For each SBM, CMAC is computed against MBEs with eigenvalues within 0.1 Hz of the SBM, because nearby eigenvalues are considered candidates for one-to-one matches. The MBEs within this frequency band will be referred to as the candidate MBEs.

1) Correspondence in Frequency and Damping: The signal-based modal analysis produces the poles visualized in Fig. 1. Close alignment in frequency and damping is observed for SBMs below 1 Hz. This is notable because the system has 4745 modes, but this spectral region remains relatively isolated. The majority of the remaining SBMs are found between 1.2 and 2.5 Hz, where they are more closely spaced with respect to frequency and damping. This leads to a discrepancy; even though there were several MBEs close in frequency and damping to the SBMs in this region, it was not clear which MBEs they corresponded to, if any.

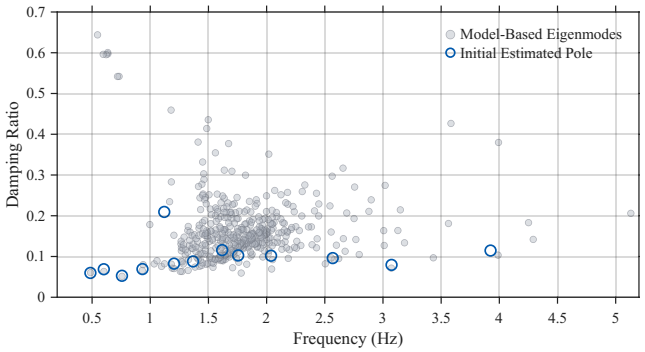

Fig. 1. Initial SBMs compared with the fixed MBE spectrum. Low-frequency SBMs are relatively isolated, while the 1 to 2.5 Hz region is more densely populated and introduces ambiguity in one-to-one correspondence.

TABLE I
Comparison of SBMs and MBEs for the Initial Disturbance

SBM (f, ζ)	Best MBE Match (f, ζ)	Best CMAC	Best Next Two CMAC Values
(0.485, 0.0597)	(0.487, 0.0604)	0.9993	0.444, 0.145
(0.601, 0.0688)	(0.601, 0.0632)	0.9773	0.0465, 0.0247
(0.757, 0.0527)	(0.757, 0.0514)	0.9983	0.0780, 0.0001
(0.933, 0.0691)	(0.931, 0.0657)	0.9395	0.1490, 0.00826
(1.12, 0.2094)	(1.034, 0.0818)	0.2215	0.1790, 0.0533
(1.20, 0.0825)	(1.204, 0.0704)	0.3318	0.0967, 0.0735
(1.368, 0.0879)	(1.336, 0.1271)	0.2168	0.1570, 0.1490
(1.612, 0.1157)	(1.708, 0.0724)	0.1966	0.0621, 0.0356
(1.755, 0.1027)	(1.781, 0.0594)	0.3546	0.2590, 0.2380
(2.038, 0.1019)	(1.967, 0.0987)	0.3875	0.1840, 0.1380
(2.567, 0.0961)	(2.504, 0.0820)	0.2117	0.1470, 0.0588
(3.074, 0.0794)	(3.072, 0.0714)	0.8596	0.0002, 0.0001
(3.924, 0.1146)	(3.989, 0.1034)	0.8267	0.0103, N/A

2) Correspondence in Mode-Shape: To provide more clarity on the SBM matches, the CMAC is evaluated between the SBM and the candidate MBEs. The mode shape vectors for the lower-frequency modes are visually observed to match in Fig. 2, and the nearby MBEs appear distinct from the best-matched MBE, both visually and by CMAC. This provides evidence that clear and distinct one-to-one matches were observed for these SBMs.

However, in regions with a dense amount of closely spaced eigenvalues, CMAC significantly drops. It does not appear that the SBMs in this region align with a single MBE. That is, while they aligned with several MBEs in terms of frequency and damping, there is no clear alignment in mode-shape. An example of an SBM in this region is pictured in Fig. 3. Both visually and in terms of CMAC, the nearby MBE eigenvectors do not resemble the SBM shape. In fact, it appeared that the signal-based approach identified a system-wide mode, while the nearby MBEs are localized and visually distinct from the SBM. Furthermore, the number of modes within each candidate MBE group around a SBM are plotted along with the best CMAC within that candidate group in Fig. 4. A relationship between closely spaced eigenvalues and poor mode-shape agreement is observed; as the number of closely spaced eigenvalues increases in a region (the number of MBEs

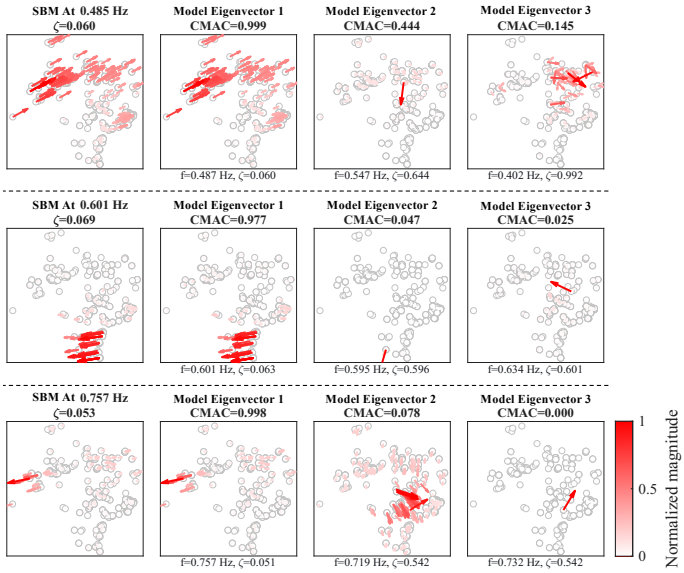

Fig. 2. The 0.485, 0.601, and 0.757 Hz SBMs align with a single candidate MBE each, in frequency, damping, and mode shape. Neighboring MBEs are visually distinct, clarifying the match between the SBMs and MBEs.

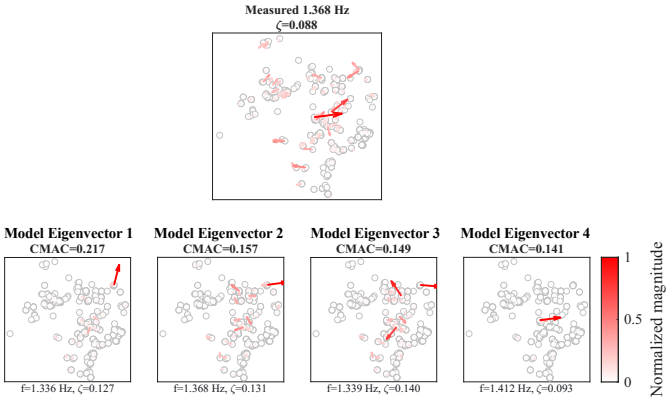

Fig. 3. Mode-shape map of an SBM at 1.368 Hz and the four candidate MBEs with highest CMAC. No candidate MBE provides a clear visual or CMAC-based match.

within the candidate MBE group), the worse the CMAC, and vice versa.

These results show that when eigenmodes are isolated via eigenvalue (frequency and damping), they can be clearly observed in the system response through a signal-based approach. However, closely spaced eigenmodes in terms of frequency and damping may limit the estimator's ability to distinguish between them. In these circumstances, a single representative SBM may reflect contributions from many underlying MBEs, as the frequency and damping were similar, yet the SBM did not align with a single MBE in terms of mode-shape.

3) Initial Validation Through Time-Domain Reconstruction: The MBEs and SBMs both reconstruct the nonlinear time-domain data with low error, even though they do not always align one-to-one. The worst-case error signal between the SBMs and the nonlinear data is pictured in Fig. 5, where the

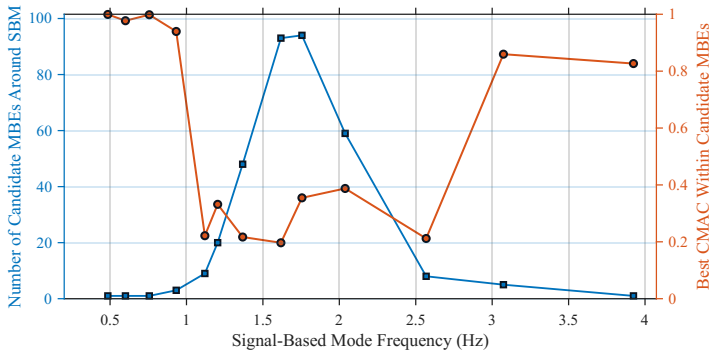

Fig. 4. The number of candidate MBEs for each SBM plotted against the highest CMAC within those candidate MBEs. Fewer candidate MBEs, and therefore less closely-spaced eigenvalues, correspond to better mode-shape alignment.

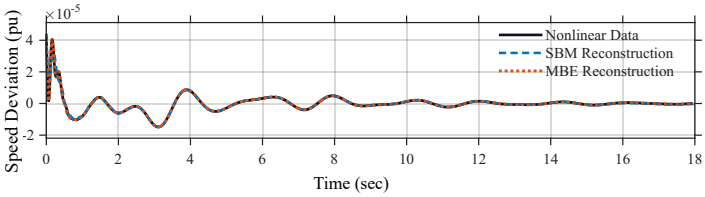

Fig. 5. The time-domain modal reconstructions plotted against the nonlinear time-domain integration data. Close alignment is shown even in the worst-fit generator-speed signal.

TABLE II
INITIAL-DISTURBANCE RECONSTRUCTION ERROR

Reconstruction Case	Average NRMSE (%)
All MBEs	0.028
All SBMs	0.066
SBMs Excluding 1.368 Hz Mode	0.535

average NRMSE is low as shown in Table II. Additionally, when the 1.368 Hz SBM is excluded, the error is 8.11 times larger on average. This indicates that this SBM was critical in the reconstruction, even though it does not match an individual MBE.

B. Varying Disturbance Location

Changing the location of the fault leads to a similar conclusion. Note that the location does not change the underlying MBEs; they remain the same as in the initial fault case. The new locations excite different MBEs to a different degree, changing the response, thereby providing an opportunity for the SBMs to change. However, note that if an SBM corresponds to a single MBE, it should not change based on the fault location.

Moving the fault location produces the results in Fig. 6. The same lower-frequency SBMs remain relatively constant across all disturbances, whereas the higher-frequency SBMs do not. The SBMs above 1 Hz are difficult to track, as sequential fault locations produce SBMs that vary widely in terms of

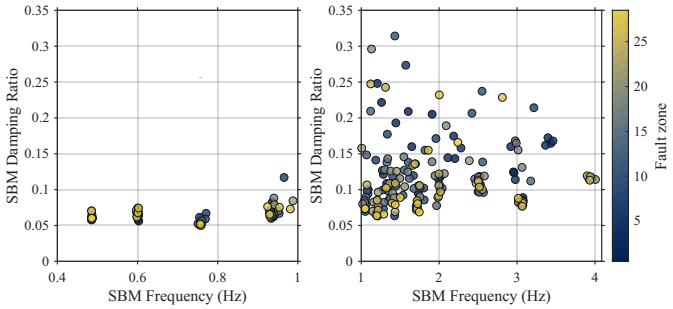

Fig. 6. Variation of identified SBM frequency and damping ratio across all fault locations, separated into (a) 0.4 to 1 Hz and (b) 1 Hz and above. Color indicates fault zone.

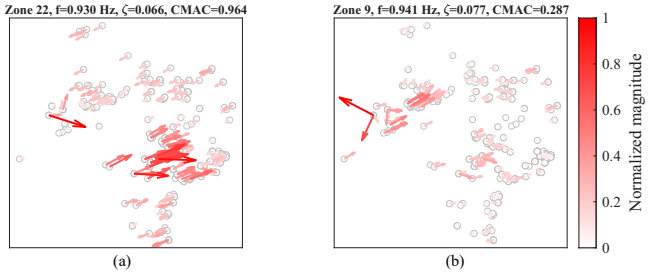

Fig. 7. SBM shape near 0.933 Hz for the fault with highest CMAC alignment in (a) and the fault with lowest CMAC alignment in (b). The change illustrates that this SBM does not consistently correspond to the same MBE across disturbance locations.

frequency and damping, and these do not align with a single MBE across the evaluated disturbances.

The mode shape of the SBM originally at 0.933 Hz in the initial evaluation also changes substantially. This is notable because in the initial set of SBMs, this particular SBM aligned well in mode shape, with a CMAC of 0.9395. However, there were many disturbances where this alignment did not occur. Fig. 7 shows the difference in measured mode shape for the closest alignment in Fig. 7a, and worst alignment in Fig. 7b. Visually, and in terms of CMAC, the mode shape vector changes considerably which reveals a discrepancy in interpreting SBM alignment with MBEs; even if an SBM has a clear match under one disturbance, it may not under another.

C. Overall Validation From Time-Domain Reconstruction

Similar to the initial disturbance, this lack of SBM-MBE correspondence is not explained by estimator fitting error or by an inaccurate set of MBEs, observed in the low reconstruction error of both to the nonlinear time-domain data across all faults. The average NRMSE is calculated across all signals in all tested faults, and the average NRMSE was 0.248% for the MBE reconstruction and 0.316% for the SBM reconstruction, similar to the initial fault results in Table II. The agreement indicates that the linearized model yielded accurate MBEs and the non-matching SBMs cannot be attributed solely to nonlinearities, because the linear model produces the same results as the nonlinear time-domain simulation.

VI. Conclusion

This paper examined the natural oscillatory modes of a large-scale power-system model, comparing modes identified through a signal-based approach with those obtained from the linearized state matrix. The analytical linearization provided the reference needed to distinguish reconstruction accuracy from agreement with the underlying eigenstructure. While some signal-based modes closely matched individual linearized eigenmodes, others did not exhibit a clear one-to-one relationship. This pattern was associated with regions where the underlying eigenvalues were closely spaced, and the discrepancies were found even when both modal representations produced accurate time-domain reconstructions. These results reveal a limitation in interpreting modes from a signal-based approach, as they can be valid reconstruction terms while not aligning one-to-one with underlying linearized eigenmodes. Future work will analyze why and when this phenomenon occurs, including under different estimator settings and in systems with inverter-based resource dynamic models.

References

[1] Western Electricity Coordinating Council, "Modes of Inter-Area Power Oscillations in the WI," Meeting document, 2024.

[2] D. J. Trudnowski, J. Follum, R. T. Elliott, D. A. Schoenwald, and J. W. Pierre, "Characterizing the oscillatory properties of bulk electric systems," *IEEE Access*, vol. 13, pp. 32 883–32 900, 2025.

[3] X. Fan, U. Agrawal, J. Follum, R. Huang, Y. Chen, and Z. Huang, "Eastern Interconnection Wide-Area Oscillation Assessment and Study Report," Pacific Northwest National Laboratory, Richland, WA, USA, Tech. Rep. PNNL-35769, Dec. 2023.

[4] H. Fu, W. Yu, M. M. Olama, N. Bhusal, A. P. Yadav, N. M. Stenvig, and Y. Liu, "Statistical analysis of inter-area oscillations in the u.s. eastern interconnection: A 2017–2023 perspective," *IEEE Access*, vol. 14, pp. 5374–5388, 2026.

[5] P. S. Kundur and O. P. Malik, *Power System Stability and Control*, 2nd ed. McGraw-Hill, 2022.

[6] T. J. Overbye, S. Kunkolienkar, F. Safdarian, and A. B. Birchfield, "On the existence of dominant inter-area oscillation modes in the north american eastern interconnect stability simulations," in *Proceedings of the 57th Hawaii International Conference on System Sciences*, Honolulu, HI, USA, Jan. 2024.

[7] W. Trinh, S. Kunkolienkar, Y. Liu, and T. J. Overbye, "On the sensitivity of ring-down observed inter-area modes in large-scale electric grids using a simulation approach," in *2022 IEEE Power and Energy Conference at Illinois (PECI)*, 2022, pp. 1–8.

[8] M. L. Crow and A. Singh, "The matrix pencil for power system modal extraction," *IEEE Transactions on Power Systems*, vol. 20, no. 1, pp. 501–502, 2005.

[9] W. Trinh, K. Shetye, I. Idehen, and T. J. Overbye, "Iterative Matrix Pencil Method for Power System Modal Analysis," in *Proceedings of the 52nd Hawaii International Conference on System Sciences*, Grand Wailea, HI, USA, Jan. 2019, pp. 1–10.

[10] P. Vacher, B. Jacquier, and A. Bucharles, "Extensions of the mac criterion to complex modes," in *Proceedings of ISMA 2010 International Conference on Noise and Vibration Engineering*, 2010.

[11] T. Xu, A. B. Birchfield, K. S. Shetye, and T. J. Overbye, "Creation of synthetic electric grid models for transient stability studies," in *Proceedings of the 10th Bulk Power Systems Dynamics and Control Symposium (IREP 2017)*, Espinho, Portugal, Sep. 2017.